Research Article

Adsorption Science & Technology
Volume 42: 1–25

DOI: 10.1177/02636174241256854
journals.sagepub.com/home/adt
Sage

Scottish softwood biochar for water remediation targeting selected persistent organic pollutants

Mohammad Umair Jamal
Department of Chemical and Process Engineering, University of Strathclyde, Glasgow, UK

Ashleigh Fletcher
Department of Chemical and Process Engineering, University of Strathclyde, Glasgow, UK

Alan Baby
Department of Chemical and Process Engineering, University of Strathclyde, Glasgow, UK

Isaac Maso
Department of Chemical and Process Engineering, University of Strathclyde, Glasgow, UK

Lidija Šiller
School of Engineering, Newcastle University, Newcastle upon Tyne, UK

Abstract

A Scottish wood biochar sample was investigated for water remediation against persistent organic pollutants as a potential renewable material for adsorption processes. Textural characterisation gave a high surface area (588 m^2/g) and a mix of microporous and mesoporous nature with an average pore width of 4 nm. Morphological analysis revealed a layered carbon structure and spectroscopic analysis showed the presence of oxygen and nitrogen-based functionalities alongside 80% atomic carbon. The biochar had an average point of zero charge

Submitted January 4, 2024; accepted April 30, 2024

Corresponding author:
Mohammad Umair Jamal, Department of Chemical and Process Engineering, University of Strathclyde, 75 Montrose Street, Glasgow G1 1XQ, UK.
Email: umair.jamal@strath.ac.uk

of 7.44 ± 0.2. 3,4-Dichloroaniline kinetic rates were rapid (<5 min), restricting kinetic analysis, while a pseudo-second-order kinetic model was best suited to represent the kinetic data for acetaminophen and carbamazepine, suggesting chemical control. The adsorption equilibria were most appropriately described by the Sips isotherm model, further supporting the chemical control theory for a multilayer system. Maximum adsorption capacity was 126 mg/g for acetaminophen removal, 40 mg/g for carbamazepine and 83 mg/g for 3,4-dichloroaniline. The biochar demonstrated good removal efficiency against all target species, showing potential as an adsorbent for water remediation.

Keywords
activated carbon, surface area, water treatment, pharmaceuticals, pesticides

Introduction

The demands on freshwater supplies to support growing populations and settlements is a key issue, particularly for communities located in water-stressed regions. Available freshwater amounts to 2.5% of total global water resources (International Energy Agency, 2017); in 2018, an estimated two billion people were living in countries experiencing water scarcity (United Nations Educational Scientific and Cultural Organization, 2021). Many also experience 'economic' water shortage, with ~1.6 million people residing in areas where water is physically available but there is an acute shortage of the required infrastructure required to access those water resources (United Nations Educational Scientific and Cultural Organization, 2021). A significant disparity exists in gathering the required water quality data, due to a lack of monitoring and reporting, especially in developing nations.

Water quality has been severely affected by pollution via natural and anthropogenic factors. On a global scale, approximately 80% of industrial and municipal wastewater is discharged into the environment without undergoing any form of treatment beforehand. The risks associated with emerging pollutants, including micropollutants, have been recognised since the early 2000s (Bolong et al., 2009). Organic pollutants can be either synthetic compounds or oxygen-demanding wastes produced from household or industrial activities. They contain compounds such as hydrocarbons, detergents, insecticides and herbicides, lubricants, endocrine disrupting chemicals (EDCs), pharmaceuticals, etc. that have detrimental effects on human and environmental health (Burton and Pitt, 2001; Verla et al., 2019). Among these, EDCs and pharmaceutical compounds are of growing concern due to release into the environment through engineered and natural pathways, without adequate monitoring systems. Such chemicals can mimic hormones within the body and interfere with the endocrine system and adversely affect bodily functions (Crisp et al., 1998). Even at low concentrations, prolonged exposure can result in adverse health effects. An EDC of particular concern is 3,4-Dicholoroaniline (3,4-DCA), a derivative of aniline with high global annual production (Livingston and Willacy, 1991) intermediate in the production of urea herbicides (Luca Tasca and Fletcher, 2017) in the synthesis of fabric pigments, and as a paint precursor (Ibrahim et al., 2021; Nurul et al., 2021). Known to be toxic to aquatic organisms and humans, with the potential to cause long-term adverse effects in aquatic environments, the predicted no-effect concentration (PNEC) for 3,4-DCA is 0.2 μg/L. In addition, the detection of Active Pharmaceutical Ingredients (APIs) in various surface waters has sparked concerns regarding their potential impact on the environment and living organisms and common pollutants in this category include acetaminophen (APAP) and carbamazepine (CBZ). APAP, commonly known

as paracetamol, is an analgesic used to mitigate moderate to severe pain (Rodriguez-Narvaez et al., 2017). Healthcare facilities, improper household disposal, inadequate treatment and veterinary treatment provided to livestock are pathways for water contamination. APAP can accumulate in the tissues of aquatic organisms, posing risks to higher trophic levels in the food chain. In humans, it has been reported to cause acute liver failure and is the second most frequent reason for liver transplantation in the USA (Larson et al., 2005). CBZ is extensively used worldwide as a multifunctional medication, serving both as an anticonvulsant and a pain-reliever (Décima et al., 2021) contamination pathways are similar to those for APAP, with a range of environmental and human health issues (Harvey, n.d.; Vaseashta, 2009) CBZ is among the emerging organic contaminants detected at the highest concentration with highest concentration (~4.6 μg/L) (Loos et al., 2013). All of these pollutant species pose a challenge for microbial degradation or decomposition in the environment, and it is necessary to develop new methods of removal from water streams; this is increasingly complex when designing systems that can target a range of species.

Photocatalytic degradation processes using biochars can target most organic pollutants including EDCs. Photocatalytic processes were used for the remediation of antibiotics and organic dyes using bismuth-based nanostructured photocatalysts. The catalysts offer the advantage of narrow bandgaps and layered structures, however, are limited in application, due to their solubility and instability at low pH, as well as issues with recovery and toxicity (Oladipo and Mustafa, 2023). The process additionally raises concerns about the formation of intermediate species, as well as capital investment, despite the advantage of the high stability offered by biochar-based catalysts (Qiu et al., 2021). Photocatalysis of 3,4-DCA, using Ti-N and Ti-S catalysts, resulted in full degradation of 3,4-DCA in 2 h at an optimal pH of 6 for Ti-N (Ellappan and Miranda, 2014). Ti-N catalysts presented a higher surface area and lower particle size compared to Ti-S catalysts. The catalyst dosage above 0.1 g/L was observed to be inversely proportional to the reaction rate. Coagulation–flocculation systems are advantageous to remove lighter particles that do not easily settle in suspension. Certain inorganic metal salts are also readily available and cheap to add to these systems. Several coagulants, however, can cause oxidation–reduction reactions in suspension and there are also possibilities of corrosion, and the production of toxic sludge, while extensive polymer usage has attracted criticism from an environmental standpoint (Iwuozor, 2019). Cost analysis of antibiotic removal using Al and Fe anodes revealed an operational cost of 0.166 US$/m^3 for a 200 mL reactor volume. Despite the process being reportedly economical, scaling up such a system, especially the fabrication of bigger reactors with higher pollutant loads would be challenging (Oladipo et al., 2022). To overcome such issues, adsorption systems using biochars have gained considerable interest. APAP removal using advanced oxidation processes has been widely studied over the years. Removal of APAP in such systems is generally instantaneous with efficiencies typically >75%. The conventional Fenton process can be modified into photo-based or electro-based processes. Both processes operate via the generation of hydroxyl radicals using UV radiation and electrodes, respectively. An investigation into the removal of 5 mM of APAP using UV radiation at 360 nm resulted in 99% removal in under 40 min (Su et al., 2013). Different electrode materials, such as Ti/boron-doped diamond and Pt sheets or gauzes have been tested for APAP removal and gave satisfactory results (He et al., 2015). Both processes can target high APAP concentrations; however, the operation of these processes requires a high capital investment due to electricity consumption (Phong Vo et al., 2019). For CBZ, the presence of electron-rich moieties makes it easier to react with strong hydroxyl radicals, and even ozone (Rizzo et al., 2019). However, the presence of other components, such as suspended solids and

organic matter, can compete for ozone, reducing the reaction efficiency (Juárez et al., 2021; Rizzo et al., 2019). CBZ removal using Fenton processes was reported to achieve a mix of removal efficiencies (Klamerth et al., 2010; Li et al., 2012; Matta et al., 2011).

Adsorption is often used as an application for targeting persistent organic compounds owing to its ease of application and the availability of a range of materials as potential adsorbents. The choice of precursor is an important step in developing an effective adsorbent material. Biochar-based adsorbents can be derived from a range of precursors and are also versatile in their field of application. They are carbon-rich by-products obtained from the pyrolysis of biomass under an inert atmosphere. They are low-cost alternatives to conventional activated carbon materials and are flexible in their field of application (Jin et al., 2022). Biochars can be ideal adsorbent materials due to their stability, high carbon content and aromatic nature and can target a range of contaminants, such as organics, heavy metals, pesticides, dyes and pharmaceuticals. Without physical or chemical activation, biochars typically are ineffective against most contaminants, primarily owing to their low surface area. With recent developments in activation techniques, however, biochar application in water remediation has provided a low-cost, low-carbon footprint alternative (Qiu et al., 2022). There is also considerable influence of the operational parameters of the system as suggested by Jin et al. (2022), who investigated the removal of Pb (II) ions using peanut shell biochars.

Quirantes et al. (2017) investigated 3,4-DCA removal using biomass fly ash and concluded that removal is regulated by boundary layer diffusion, while strong adsorbate–adsorbent interactions have been observed (Bakhaeva et al., 2001; van Oss, 2007). APAP adsorption appears to be controlled by the hydroxyl and amino functional groups acting as electron donors, augmenting the electron density on the aromatic ring (Pauletto et al., 2021), which may be influenced by the surface groups present on the biochar surface (Tran et al., 2020). CBZ, on the other hand, is reported to interact through mechanisms including chemical bonding, π–π interaction, and Lewis acid–base interaction; and despite its weak hydrogen bonding, CBZ has been shown to chemical bond with biochar surfaces (Liang et al., 2020). Enrofloxacin removal was investigated using biochar derived from cow dung, modified under three different phosphoric acid concentrations (10%, 30% and 50%). Largest surface area was reported for 30% phosphoric acid modification, which also coincided with the maximum adsorption capacity of enrofloxacin at 63.61 mg/g (Jiang et al., 2024). This indicates that, despite all being aromatic molecules, there is a range of interactions between these target molecules and a potential adsorbent material.

Despite compelling concepts and innovation for the use of biochar, market demand and large-scale application require ample supply of feedstock and significant capital input for process application. A comprehensive production technique could lead to smaller profit margins providing a challenge in gaining capital investments. Companies and manufacturers often tend to evaluate these risk factors to ensure the accessibility of a final product that is reasonably priced and user-friendly. The aim of this work is to investigate the removal of 3,4-DCA, APAP and CBZ from an aqueous system using biochar derived from native Scottish woods, analysed using thermodynamic and kinetic studies. Locally procured raw material provides a considerable reduction in carbon footprint associated with supply and transport, offering the potential for circularity in the formation of biochar materials for possible applications.

Materials and methods

The precursor used for making the biochar was procured from Sustainable Thinking Scotland C.I.C. (Kinneil Estate, Bo'ness, Scotland). Wood samples are taken from deforested wood in the walled garden of the 200-acre estate. The sample

mix was pure softwood including species such as Scots pine, western red cedar, and Sitka spruce.

Pyrolysis

Previous results (Jamal and Fletcher, 2023) indicated that, for the feedstock used, the optimum yield and surface area were obtained for a sample pyrolysed at 725 °C, with a hold time of 60 min and a heating rate of 15 °C/min (known as the optimised biochar). Before pyrolysis, wood samples were divided into small cubes, rinsed with DI water and oven-dried for 24 h at 100 °C. A precursor weight of 30 ± 0.1 g was distributed into three crucibles with a lid placed on top and pyrolysed inside a Thermconcept KLS 10/12/WS muffle furnace. An inert atmosphere was obtained inside the furnace using a CO_2 flow rate of 250 mL/min. The furnace was switched on at the designated temperature and dwell time conditions and at the end of each run, the flow of gas was switched off and samples were allowed to cool overnight before analysis. Figure 1 shows a schematic diagram of the muffle furnace used in this study.

Biochar production was repeated twice to ensure the results fell within acceptable error margins.

Material characterisation

Porous structure characterisation. Biochar-specific surface area and pore size distribution were determined using Brunauer–Emmett–Teller (BET) (Brunauer et al., 1938) and Barrett–Joyner–Halenda (BJH) (Barrett et al., 1951) models. Samples were crushed to a powdered form before analysis. A Micromeritics ASAP 2420 system was used to perform nitrogen adsorption at −196 °C. Sample degassing was performed at 200 °C for 4 h at a heating rate of 10 °C/min. The adsorption branch of the isotherm consisted of 49 points, with 30 points on the desorption branch.

Fourier transform infrared spectroscopy (FTIR). Attenuated Total Reflectance (ATR) was used to study functional groups on the biochar surface. A small amount of powdered biochar was analysed using an ABB IR Instrument MB3000 series. The acquisition mode was set to transmittance, with a detector gain of 80% for increased accuracy. A total of 32 scans were taken between wavenumbers 500 and 4000 cm^{-1}, at 4 cm^{-1} resolution.

X-ray photoelectron spectroscopy (XPS). XPS analysis was used to determine the surface chemistry of the biochar sample and was performed by the NEXUS facility. The biochar sample was crushed to a powdered form and analysed using a K-Alpha Photoelectron Spectrometer (Thermo Fisher) and electron detection using a hemispherical analyser. Measurements were taken with the flood gun on to lower charging with the beam energy at 40 eV and a step size of 0.05 eV. The generated results were analysed using the Fityk programme.

Point of zero charge (PZC). PZC analysis was performed using a salt addition method (Bakatula et al., 2018). A 40 mL portion of a solution containing 0.1 M $NaNO_3$ was modified to reach five different pH levels ranging from 3 to 11. To achieve the desired pH, solutions of 0.1 M NaOH and 0.1 M HCl were utilised. Approximately 0.2 g of powdered biochar was introduced into the beakers and stirred at a speed of 450 rpm for 24 h. The resulting mixture was filtered, and the pH of the filtered liquid was measured. By calculating the difference between the initial and final pH values of the samples and plotting the change in pH against the initial value, the PZC value was determined.

Scanning electron microscopy (SEM). Scanning electron microscopy (SEM) of biochar samples was performed to examine surface structure and morphology. Surface imaging of biochars produced in this work was performed by clipping a small solid portion from the material and placing it into a Tungsten low-vacuum JEOL JSM-IT100 InTouchScope SEM. Images were captured at 10 μm with

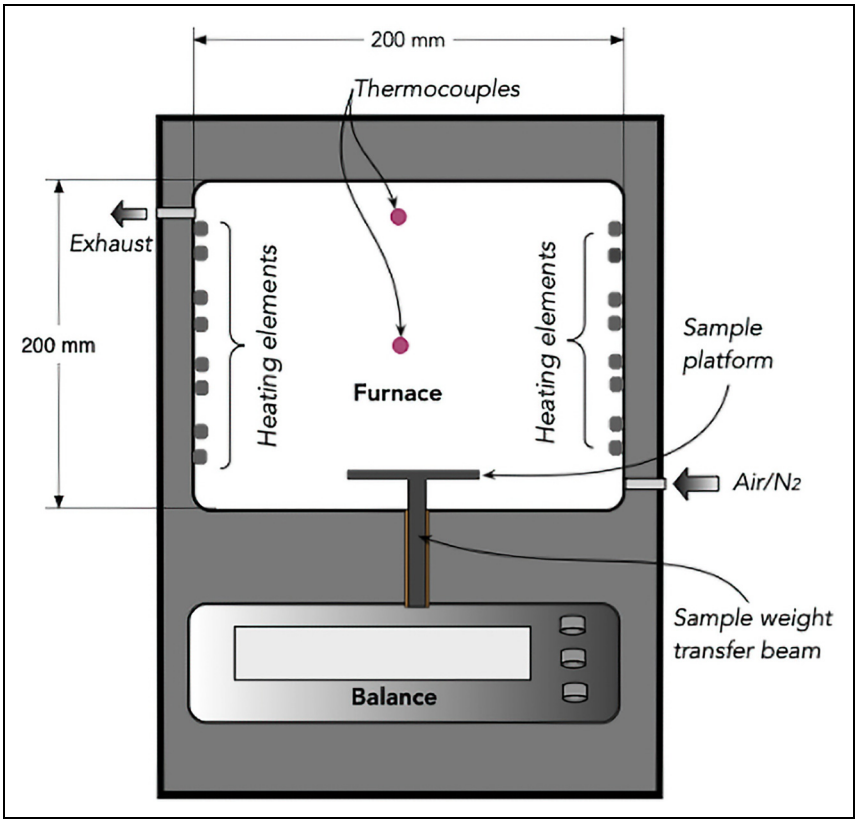

Figure 1. Schematic diagram of muffle furnace equipped with a weighing system (Licence number: 5501811254585) (Cao et al., 2021).

1000× magnification. The beam current was kept constant at 35 with a voltage difference of 20 kV.

Analytical method

The experimental solutions were passed through Fisherbrand Grade 601 general-purpose filter papers (125 mm diameter). Two filter papers were used for each filtration step to ensure the removal of all suspended particles from the permeate. For the target species in this work, calibration curves were plotted prior to kinetic and adsorption experiments. The maximum adsorption wavelengths for 3,4-DCA, APAP and CBZ are 296, 243 and 285 nm, respectively. For calibration, absorbance obtained by passing light of monochromatic radiation was plotted against concentration and a liner fit provided the required parameters of slope and intercept. The generated equation was then used to identify residual concentrations from experimental runs.

Adsorption kinetics

Biochar samples (0.1 g) were added to 100 mL glass bottles and mixed with 50 mL of 100 mg/L solution of either APAP, CBZ or 3,4-DCA. The bottles were subsequently placed on an orbital shaker at 420 rpm for time steps 15, 30, 60, 120, 180, 240, 360 and 1440 min. Once completed, the solutions for each time step were double-filtered using cellulose

acetate filter papers to obtain a clear solution free of suspended biochar particles. The supernatants were analysed using UV-Vis spectroscopy. The amount of target species adsorbed was calculated using calibration curves run prior to kinetic and isotherm measurements. It should be noted that there was an exception in the case of 3,4-DCA kinetic analysis. The speed of adsorption was observed to be extremely fast, not allowing sufficient time to measure and analyse multiple samples. Hence, a reduction in temperature was used, using an ice bath (~2–3 °C) to slow the reaction process to obtain kinetic parameters. A series of kinetic models were applied to determine the most appropriate fit.

The pseudo-first-order (PFO) model was first proposed by Lagergren in 1898 (Svenska Vetenskapsakademiens, n.d.). The differential form of the model is given by Equation 1:

$$\frac{dq_t}{d_t} = k_1(q_e - q_t) \tag{1}$$

where k_1 is the rate constant for adsorption, and q_e and q_t are the adsorbate uptake amounts at equilibrium and a given time 't', per mass of adsorbent, respectively. Integrating the above equation provides the linearised form of the model shown in Equation 2 (Moussout et al., 2018):

$$\ln(q_e - q_t) = lnq_e - k_1 t \tag{2}$$

Which upon rearranging gives the non-linear PFO model given by Equation 3:

$$q_t = q_e(1 - e - k_1 t) \tag{3}$$

The physical meaning associated with the model has been suggested to be dependent on the initial solute concentration (Azizian, 2004; Liu and Shen, 2008). The PFO model is associated with a high initial solute concentration, the process being at the initial stage of adsorption, and the availability of only a few active adsorbent sites (Wang and Guo, 2020b).

Ho and McKay (1998) proposed the expression for the pseudo-second-order (PSO) model by integrating Equation 4:

$$\frac{dq_t}{d_t} = k_2(q_e - q_t)2 \tag{4}$$

And applying it to the adsorption of lead onto peat, to obtain the non-linear model displayed in Equation 5:

$$q_t = \frac{q_e 2k_2 t}{1 + q_e k_2 t} \tag{5}$$

where k_2 is the reaction rate constant, and all other terms are as defined for PSO. The linearised form of the model is given as shown in Equation 6:

$$\frac{t}{q_t} = \frac{1}{k_2 q_e 2} + \frac{t}{q_e} \tag{6}$$

PSO models are more commonly used to predict adsorption experiments as opposed to PFO models. The model signifies a low initial solute concentration, occurring within the final stages of the adsorption process, and an abundance of active sites on the adsorbent (Wang and Guo, 2020b).

Adsorption isotherms

Batch adsorption experiments were carried out using 0.1 g biochar in 50 mL solution of the target species. For APAP and 3,4-DCA, the concentrations used were 25, 50, 75, 100, 150, 200, 250 and 300 mg/L. For CBZ, the maximum solubility is 125 mg/L and, hence, the isotherm points were taken between 10 and 100 mg/L at intervals of 10 mg/L. Based on the kinetic data, 3,4-DCA isotherm solutions were filtered after 10 min. Experiments for APAP were run for 6 h and CBZ experiments were allowed to run for 24 h to allow for full equilibration of the samples. The permeate collection procedure was similar to that used within the kinetic measurements, where the solutions were double-filtered using two cellulose acetate filter papers, and the absorbance was measured using UV-Vis spectroscopy.

The collected isotherm data was analysed using three adsorption isotherm models.

The non-linear form of Langmuir model (Langmuir, 1916) is given in Equation 7:

$$q_e = \frac{q_m K_L C_e}{1 + K_L C_e} \tag{7}$$

where q_m is the maximum adsorption capacity in mg/g, C_e is the equilibrium concentration of the solute in mg/L, q_e is the amount of solute adsorbed in mg/g and K_L is the ratio between adsorption and desorption rates in L/mg. The model represents a chemical adsorption process with monolayer formation and homogenous adsorption (Wang and Guo, 2020a).

The Freundlich model (Freundlich, 1907) is given in Equation 8:

$$q_e = K_F C_e^{1/n} \tag{8}$$

where K_F is the rate constant in $L^{1/n}mg^{1-1/n}/g$ and n is a correction factor. The linearised form of the model can be obtained when $n = 1$. All other terms are as defined above. This model represents nonlinear adsorption processes and can be treated as an empirical equation (Wang and Guo, 2020a).

The Sips model (Sips, 1948) is often referred to as the Langmuir–Freundlich isotherm model and was developed in 1948. The non-linear form is shown in Equation 9:

$$q_e = \frac{q_{ms} K_s C_e^{ns}}{1 + K_s C_e^{ns}} \tag{9}$$

where the maximum adsorbed amount is represented by q_{ms} in mg/g and K_S ($L^{ns}.mg^{-ns}$) and n_S are the Sips constants. When the value of n_S in the Sips model is equal to 1, the model simplifies to the Langmuir model. At low initial concentrations (C_0), the Sips model also resembles the Freundlich model. However, it is important to note that, unlike the Sips model, the Langmuir model satisfies Henry's law at low C_0. The model can be applied to homogeneous as well as heterogeneous systems and describes the adsorption process of a monolayer, where one adsorbate molecule is adsorbed onto $1/n_S$ adsorption sites (Wang and Guo, 2020a).

Results

Material characterisation

Figure 2 shows the adsorption–desorption isotherms obtained for the optimised biochar sample. The adsorption isotherm shows a high initial uptake at low relative pressures, followed by a plateau in the high relative pressure region, which can be attributed to the microporous and mesoporous nature of the material. This resembles a Type IV isotherm behaviour, as per the IUPAC classification of physisorption behaviour (Thommes et al., 2015). The desorption branch between the pressure range 0.85–0.4 shows the hysteresis loop which typically results from the presence of mesoporosity in porous materials. The difference in desorption branch can be linked to differences in evaporation mechanisms, cavitation and pore blocking.

The hysteresis loop resembles Type H4 where the adsorption branch is associated with micropore filling at low relative pressures as expected for microporous carbons (Thommes et al., 2015), this is further supported by the ratio of micropore to total pore volume for the biochar sample, which was 55%. The micropore volume was calculated using the t-plot method developed by Lippens and Boer (Lippens and de Boer, 1965). Total pore volume (TPV) was calculated using Equation 10:

$$TPV = \left(Q_{sat} \times \frac{M_W}{V_m}\right) / \rho_{liq} \tag{10}$$

where Q_{sat} is the maximum nitrogen adsorption in cm^3/g, MW is the molecular weight of nitrogen (28 g/mol), V_m is the volume occupied by 1 mol of gas (22.4 L) and ρ_{liq} is the density of nitrogen at boiling point (808 g/L). TPV of the biochar sample was 0.36 cm^3/g with an average pore width of 4 nm, and the pore volume distribution is shown in Figure 3. It is evident from the distribution that the produced

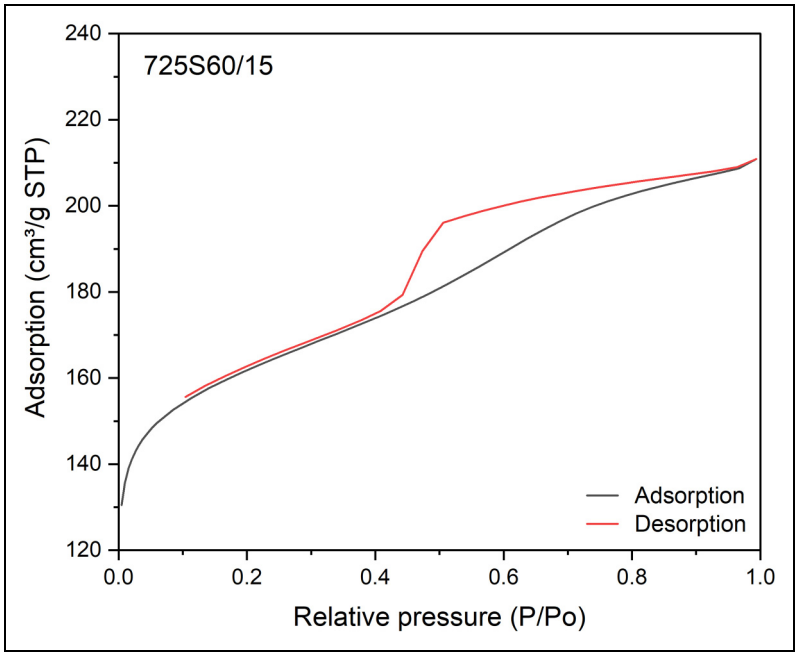

Figure 2. Nitrogen adsorption and desorption isotherms on the optimised biochar sample.

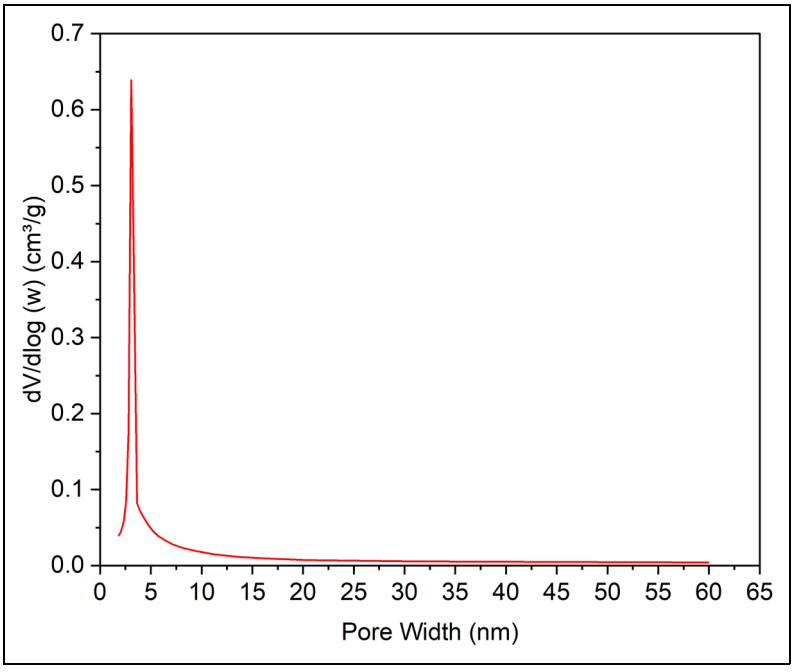

Figure 3. Pore volume distribution of the optimised biochar sample using BJH method (Barrett et al., 1951).

biochar material is highly microporous with a discrete pore size.

The biochar surface area was calculated, using the BET method, to be 620 m^2/g. BET analysis, however, is sensitive to the selected relative pressure region (Gómez-Gualdrón et al., 2016); specifically for microporous materials, the optimal range of relative pressure can be determined by applying the four consistency criteria proposed by Sing (2014). These criteria are as follows: (1) only the range where the product of the adsorbate loading rate and the difference between 1 and the relative pressure exhibits a monotonic increase with the relative pressure should be selected; (2) the value of the BET 'C constant' should be positive. The C constant represents the interactions between the adsorbent and adsorbate and is linked to the energetic aspects of the first adsorbed layer (Gómez-Gualdrón et al., 2016); (3) the linear region chosen should include the loading corresponding to the monolayer at the given relative pressure; (4) the relative pressure obtained from Criterion 3 should be within a 20% tolerance of the relative pressure calculated from BET theory that aligns with monolayer loading. Upon applying the correction to the data obtained for this biochar sample, the 'corrected' surface area was calculated to be 588 m^2/g, which is larger than other wood-based biochars reported in previous studies (Idowu and Fletcher, 2020; Jindo et al., 2014; Kloss et al., 2012).

The FTIR spectra obtained for the wood feedstock and the optimised biochar are shown in Figure 4. The fingerprint region, observed between 600 and 1500 cm^{-1} shows the presence of vinyl terminals (Nandiyanto et al., 2019). At 1000 cm^{-1}, there is evidence of a loss of the peak observed in the feedstock, due to heat treatment. The peak loss can be attributed to the removal of C-OH vibrations from dehydration during pyrolysis (Idowu and Fletcher, 2020). The process of heat treatment is essential in facilitating condensation of the carbonaceous skeleton and eliminating the hydroxyl groups found in the cellulosic compounds within the initial materials (Lee et al., 2010). Overall, the feedstock and biochar spectra look comparable with the presence of C = C bonds with symmetric and asymmetric vibrations between 1600 and 1800 cm^{-1}.

The XPS spectra of the optimised biochar sample used are shown in Figure 5. The spectra show the presence of oxygen and nitrogen bonds, in addition to carbon with peaks at 532.5, 400 and 284.5 eV, respectively (Reddygunta et al., 2022). Peak deconvolution was achieved using the Fityk programme, and the Voigt function assisted in the identification of the heteroatoms present in the biochar. The corresponding parameters are provided in Table S1 (Supporting Information). C1s peaks were deconvoluted into three peaks at 284.5 eV, suggesting a graphene-like arrangement (C = C), at 285.6 eV indicating the presence of carbonyl bonds (C-O), and a third peak at 289.6 eV, which is ascribed to either carboxylic or pyridinic N bond functionalities (C = O/C-N) (Beamson and Briggs, 1992; Lhoest et al., 1995; Smith and Black, 1984; Wagener et al., 1989). The area under the C = C peak is the largest indicating the preservation of the graphene-like arrangement in the wood samples post-pyrolysis. Peak convolution of O1s showed the presence of both carbonyl, as well as carboxyl groups, with peaks at 531.1 and 532.9 eV (Beamson and Briggs, 1992; López et al., 1991). There were also trace amounts of nitrogen functionalities present in the sample and convolution of the N1s spectra suggested the presence of pyridinic (398.6 eV) as well as graphene N (400.2 eV) bonds in the sample (NIST X-ray Photoelectron Spectroscopy (XPS) Database, Version 3.5, n.d.). The incorporation of O and N-based functional groups into the carbon framework enhances its wettability (Reddygunta et al., 2022), which is further correlated with contact angle measurement presented in previous work (Jamal and Fletcher, 2023), where biochar samples proved to be extremely hydrophilic. The calculation of the elemental compositions of C, N and O were performed as

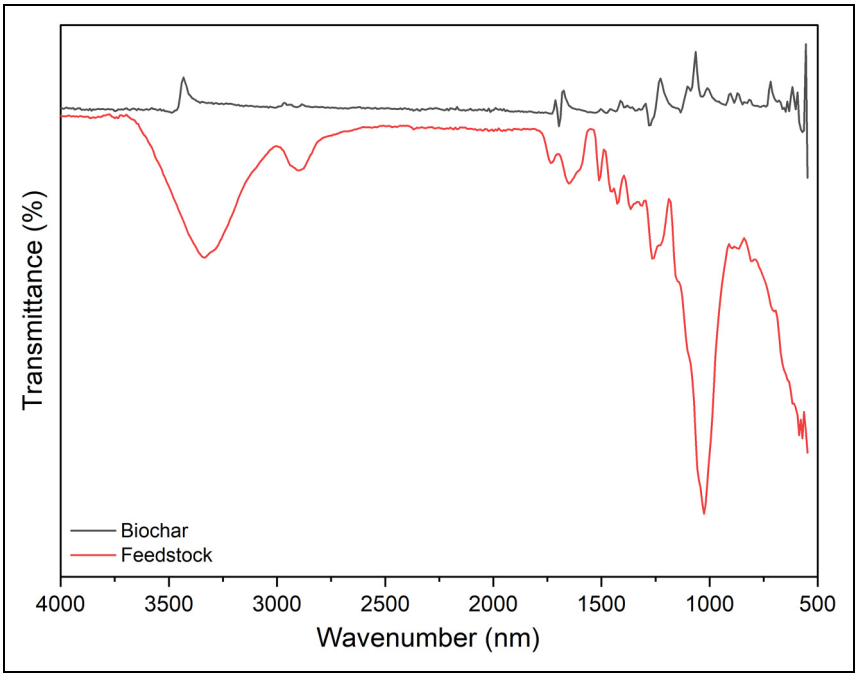

Figure 4. FTIR spectra of wood feedstock and biochar.

suggested by Alexander G. Shard (Shard, 2020). Equation 11 works under the assumption that the sample is homogenous and a single phase within the penetration depth; where X represents the atomic fraction (in %), and I_P/S_P is the intensity divided by the sensitivity factor ($S_P = 1$, 1.8 and 2.93 for C, N and O, respectively).

$$X = \frac{IP / SP}{\sum_j Ij / Sj} \tag{11}$$

The biochar sample used consisted of 80% C, 13% O and 7% N fractions. The findings again supplement the results obtained in the previously reported study, where thermogravimetric analysis of the samples showed 80% fixed C (Jamal and Fletcher, 2023).

The PZC of the biochar was observed to be 7.44 ± 0.2. The results are comparable to the previous study on parameter optimisation, where the DOE biochars had similar average PZC values (Jamal and Fletcher, 2023). PZC values are temperature dependent, and high temperatures result in a loss of volatile matter including acidic functional groups such as phenols and carboxyl, causing the resulting biochar to have a more alkaline nature (Shaheen et al., 2019). PZC of wood pellet biochars was also reported to increase with increasing temperatures (Zhang et al., 2015); such alkaline/neutral PZC values make these biochars suitable for potential application in drinking water systems that operate naturally under slightly acidic conditions.

Figure 6(a)–(d) shows the SEM images recorded for lower ramp rate biochars and Figure 6(e)–(h) displays the observations for higher ramp rate biochars. There is evidence of a well-developed pore network in biochars produced at both ramp rates. The images at 10 µm and 1000× magnification suggest that the high pyrolysis temperatures used to create the biochars exposed the carbonaceous skeleton of the parent material encompassing an intricate network of pores (Angın, 2013). A pyrolysis

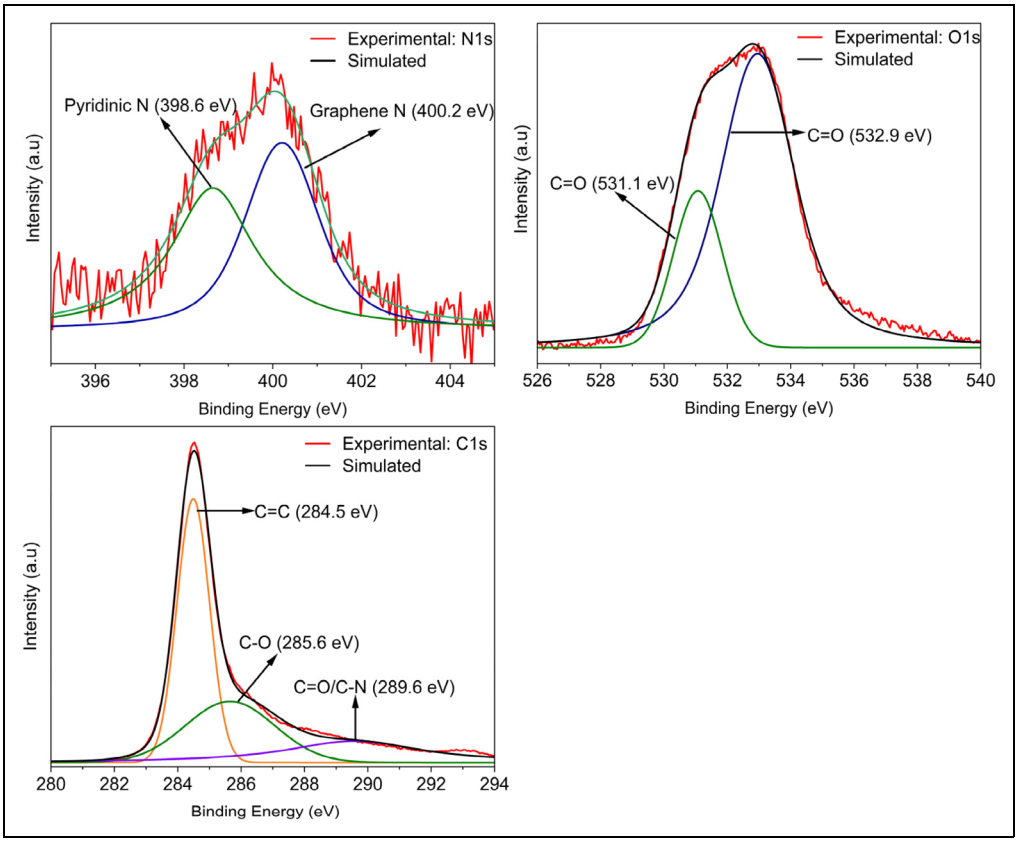

Figure 5. XPS spectra and Fityk simulated models showing N1s, O1s and C1s scans. Fityk models suggest possibilities of existing functional groups at specific binding energies that can be compared with the NIST database.

temperature that is sufficiently high is necessary for the removal of the outer biochar layer. The open structure of pores could be attributed to a lower ash content, which reduces the potential for clogging. There is no apparent evidence of influence from different ramp rates on the pore networks developed in the biochars.

Adsorption kinetics

Table 1 shows the parameters of kinetic models fitted to the data obtained for adsorption of APAP and CBZ onto the optimised biochar. Kinetic analysis of 3,4-DCA revealed fast adsorption rates, which could not be fitted to any kinetic models.

Data was obtained for 3,4-DCA adsorption on the optimised biochars at room temperature, for an initial concentration of 100 mg/L. Removal was observed to be 90% after 15 min, with a plateau thereafter. Readings were, therefore, taken at shorter time intervals, and also at lower temperature in an attempt to slow the kinetic process. Table 2 shows the removal percentages of 3,4-DCA at room temperature and in the ice bath. The data obtained confirms the rapid adsorption of 3,4-DCA onto the optimised biochar, even at the lower temperature, hence, it was not possible to monitor the adsorption in order to determine the kinetic parameters for 3,4-DCA.

The results indicate that the interaction between the biochar surface and 3,4-DCA molecule is almost instant. An investigation into solution pH also yielded similar results with

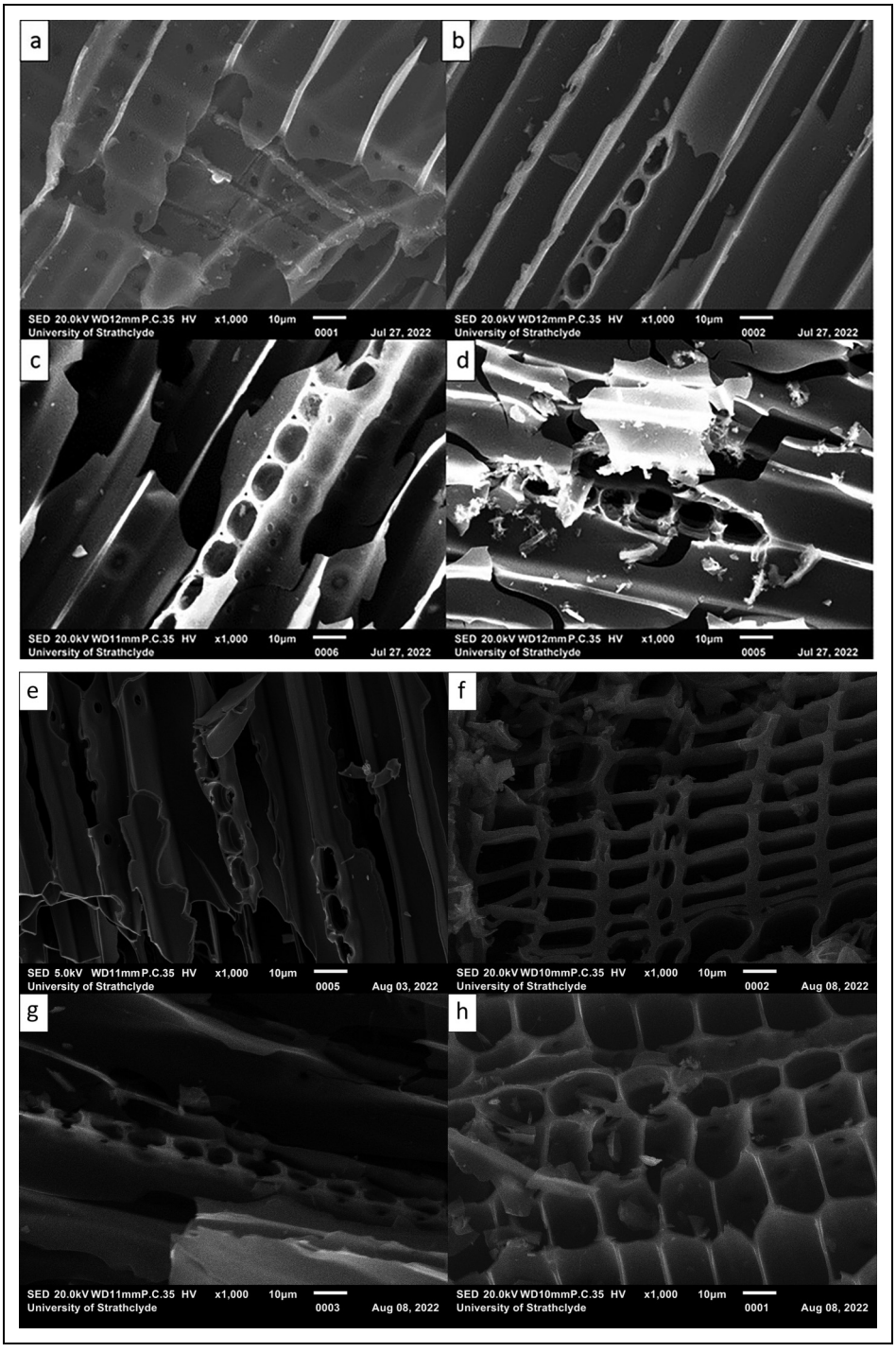

Figure 6. SEM images biochar material ($T = 725$ °C). (a, b) 60 min at 15 °C/min; (c, d) 20 min at 15 °C/min; (e, f) 60 min at 30 °C/min; (g, h) 20 min at 30 °C/min.

Table 1. Kinetic parameters of adsorption models fitted to Acetaminophen (APAP) and carbamazepine (CBZ).

Model parameters	APAP	Carbamazepine
Pseudo first order (non-linear)		
R^2 (COD)	0.461	0.460
Adjusted R^2	0.371	0.371
χ^2	0.678	9.921
q_e (mg/g)	46.72 ± 0.315	38.83 ± 1.266
K_1 (min^{-1})	0.207 ± 0.028	0.097 ± 0.023
Pseudo second order (non-linear)		
R^2 (COD)	0.871	0.782
Adjusted R^2	0.849	0.746
χ^2	0.162	4.004
q_e (mg/g)	47.32 ± 0.199	40.56 ± 1.001
K_2 (g/mg × min)	0.021 ± 0.003	0.004 ± 0.001
Pseudo second order (linear)		
R^2 (COD)	1	1
Adjusted R^2	1	1
χ^2	–	–
q_e (mg/g)	47.62	46.86
K_3 (g/mg × min)	0.013	0.054

Table 2. Biochar performance against 3,4-DCA at room temperature and in an ice bath.

Time (min)	% Removal -> room temp.	% Removal -> 3 ± 0.5°C
2	94	86
4	94	88
6	95	90
9	95	89

overnight runs at pH 6 and 9 resulting in 93% and 91% removal, respectively. Previous research into 3,4-DCA removal using adsorption suggested that the data followed a pseudo-second-order kinetic model (Angioi et al., 2005). The observed reaction rates in this study are quicker than those previously reported. Experiments using kaolinite and montmorillonite to test the removal of chloroanilines, including 3,4-DCA, were reported to achieve equilibrium in under 4 days (Polati et al., 2006). Another study into 3,4-DCA removal from water using biomass fly ashes reported kinetic equilibrium at approximately 10 h (Quirantes et al., 2017). A selection of low-cost materials including corncob char, sugar beet pulp, perlite, and vermiculite were also tested against 3,4-DCA. The quickest reaction time to achieve maximum sorption percentage was 60 min using vermiculite (Huguenot et al., 2010). The rates observed here indicate that there is significantly quicker adsorption for the biochars created in this work.

Figure 7 shows the kinetic data obtained for the sorption of CBZ and APAP on the biochar sample. Sorption kinetics for APAP showed rapid uptake with 90% removal achieved in 15 min followed by a gradual increase in the uptake, and equilibrium achieved after approximately 2 h. For CBZ, the uptake was slower with just under 75% removal at 15 min and adsorption slowed considerably after 2 h, with equilibrium achieved after 24 h.

The linearised pseudo-second-order rate equation showed a better fit for the data for both species compared to pseudo-first-order and non-linear second-order kinetic models (Table 2). The adjusted R^2 values for both species were$\geq$0.99. The maximum adsorption capacity for APAP was 47.6 mg/g and 46.7 mg/g for CBZ. The second-order rate constants show a quicker uptake rate for APAP than CBZ with the adsorption rate being 0.013 g/mg × min. The high R^2 values obtained for both species, with linear PSO model fitting, can be attributed to the availability of abundant vacant active sites in the physically activated biochar and the adsorption process being ruled by chemisorption (Abd et al., 2020; El Saied et al., n.d.; Wang and Guo, 2020b). The mechanism could likely be attributed to hydrogen bonding between the species. Additionally, π–π interactions between the benzene ring in APAP and CBZ and the aromatics in biochar can influence the adsorption process (Abd et al., 2020).

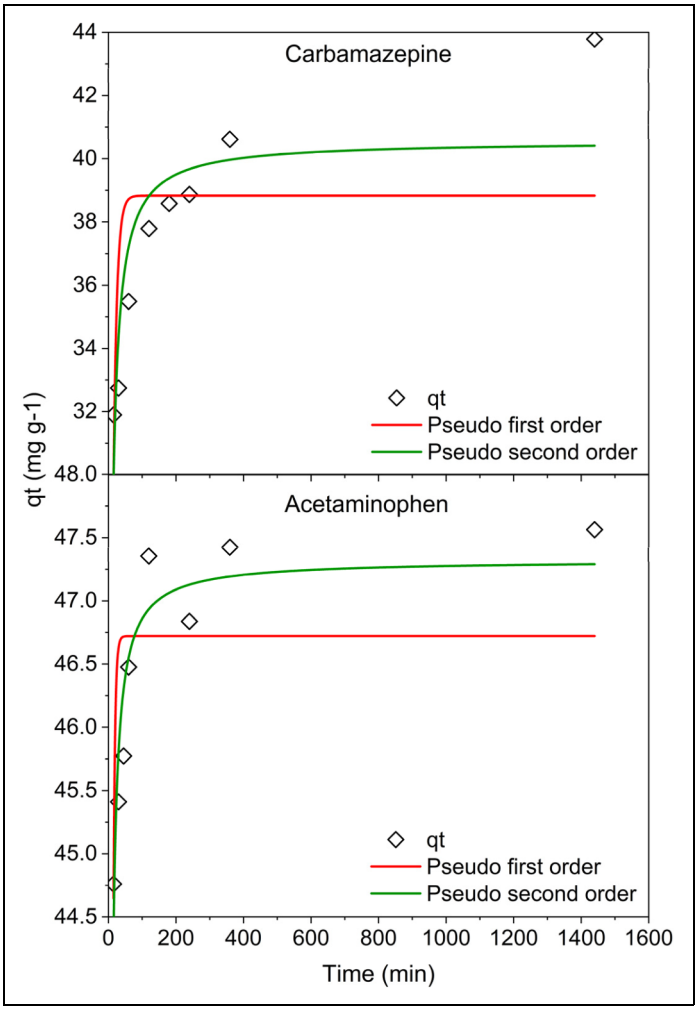

Figure 7. Non-linear kinetic model fittings for (top) carbamazepine and (bottom) acetaminophen on the optimised biochar showing fits for pseudo-first-order and pseudo-second-order models.

Further analysis of the kinetic data was performed using the intraparticle diffusion model proposed by Weber and Morris (Weber and Morris, 1963), to understand the rate-controlling step in the adsorption process. The model equation is given below:

$$q_t = kpt^{1/2} + C \tag{12}$$

where k_p is the intraparticle diffusion rate constant in mg/g·min$^{1/2}$ and C is a constant that represents the boundary layer effect and initial adsorption. Linearised plots of the model are depicted in Figure 8.

The plots suggest that the adsorption process for both pharmaceutical species involved three diffusion steps. In both cases, liquid film diffusion was the dominating phase signifying rapid diffusion of molecules onto the active sites in the pores and voids of the biochar (Wang et al., 2021; Zhao et al., 2022). There is a hint of intraparticle diffusion in CBZ adsorption. This step involves the gradual diffusion of molecules into the micropores before the

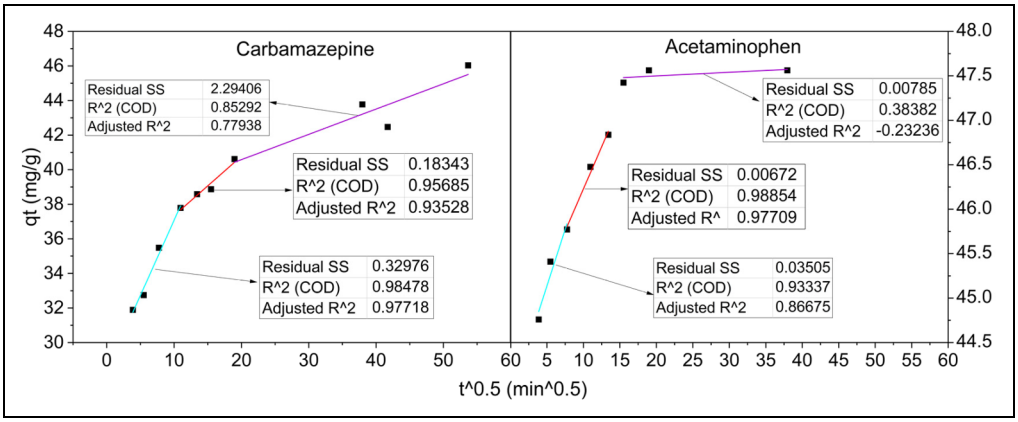

Figure 8. Intraparticle diffusion model fittings for acetaminophen and carbamazepine adsorption show three steps of the diffusion mechanism.

reaction proceeds to the equilibrium stage. For APAP however, the intraparticle diffusion phase is not as prevalent and the reaction appears to proceed rapidly to equilibrium after liquid phase diffusion. This also correlates with the longer time required by CBZ to reach equilibrium compared to APAP. The three target molecules have some similarities, allowing a comparison of their adsorption behaviour relative to their chemistry. All contain amine functionalities and benzene rings, with APAP/BBZ sharing carbonyl moieties and only 3,4-DCA containing halogenated species. The slower kinetics for CBZ could realistically be a consequence of the significantly larger relative size of the molecule (see Supporting Information), while the rapid adsorption of 3,4-DCA is likely a result of the comparatively increased electrostatic interactions, where the chlorine groups will be electron withdrawing from the benzene ring.

Adsorption isotherms

Adsorption isotherms are of crucial importance in determining the maximum adsorption capacity of the adsorbent and understanding the adsorption equilibrium. The results of isotherm fittings for the Langmuir, Freundlich and Sips models are given in Table 3, and isotherm plots for the target species are shown in Figure 9.

The results indicate that the adsorption uptake was significant at low pollutant concentrations. The data presented in Table 3 suggests that for CBZ and 3,4-DCA, the Sips model can be best used to describe the adsorption behaviour. This suggests that the adsorption process is a combination of physisorption at low concentrations and chemisorption at high initial C_o values with the formation of a monolayer on the adsorbent material. The maximum adsorption capacities for CBZ and 3,4-DCA, suggested by the Sips model, were 39.8 mg/g and 83.2 mg/g, respectively. For APAP, both Langmuir and SIPS isotherm models demonstrated high R^2 values with the chi-square value lower in the case of Langmuir isotherm. A good fit to the Langmuir model assumes monolayer adsorption of the molecules on the biochar surface, with almost identical activation energies, albeit with the possibility of multilayer formation (El Saied et al., n.d.). The maximum adsorption capacity for APAP is determined as 126 mg/g, much higher than the other two species, which may be reduced as a consequence of molecular size affecting packing in the case of CBZ and electrostatic

Table 3. Adsorption isotherm parameters obtained for Acetaminophen (APAP), carbamazepine (CBZ) and 3,4-dicholoroaniline (3,4-DCA) on the optimised biochar sample.

Isotherm parameters	APAP	CBZ	3,4-DCA
Langmuir			
R^2 (COD)	0.976	0.907	0.905
Adjusted R^2	0.972	0.895	0.893
χ^2	47.46	23.58	112.5
q_m (mg/g)	118.9 ± 5.910	59.84 ± 9.694	110.9 ± 15.36
K_L (L/mg)	0.204 ± 0.036	0.182 ± 0.065	0.028 ± 0.010
Freundlich			
R^2 (COD)	0.929	0.801	0.797
Adjusted R^2	0.915	0.772	0.769
χ^2	105.1	40.16	200.3
q_m (mg/g)	32.62 ± 4.966	11.77 ± 2.679	9.771 ± 4.409
K_F ($L^{1/n}mg^{1-1/n}/g$)	0.313 ± 0.044	0.503 ± 0.106	0.456 ± 0.104
SIPS			
R^2 (COD)	0.977	0.968	0.939
Adjusted R^2	0.967	0.959	0.922
χ^2	55.22	9.24	81.64
q_m (mg/g)	126.2 ± 19.81	39.77 ± 2.105	83.20 ± 7.025
K_S ($L^{ns} \cdot mg^{-ns}$)	0.214 ± 0.046	0.065 ± 0.032	0.002 ± 0.003

repulsion in the case of 3,4-DCA due to overlapping of the electron clouds of the molecule within the pore structure (Weber, 1974).

Since the two models exhibited a good fit to the experimental data for APAP, the value of the separation factor (R_L) suggested by Webber and Chakkravorti (Weber and Chakravorti, 1974) was calculated to further verify the favourability of the Langmuir adsorption isotherm (see Supporting Information). The separation factor is determined from Equation 13:

$$R_L = \frac{1}{1 + K_L C_o} \tag{13}$$

The value for RL was >1 for all Co values suggesting unfavourable adsorption (Wang and Guo, 2020a). However, this could also be attributed to the limitations of the model assumptions, including homogenous adsorption sites and identical adsorption energies. The model is also limited to the assumption of monolayer adsorption, which can be overcome by the Sips model, which includes the possibility of multilayer formation. To conclude, APAP adsorption on the biochar surface is better represented by the Sips model (Wang and Guo, 2020a).To further investigate the nature of adsorption sites, Scatchard plots were obtained from the adsorption data. The Scatchard equation is given in Equation 14.

$$\frac{q_e}{C_e} = Q_b - q_{eb} \tag{14}$$

where the Scatchard adsorption constant Q is in mg/g and b is in L/mg. The nature of the material surface can be interpreted from the plot between q_e/C_e vs. q_e. If the plot is linear, the material surface is expected to be homogeneous with a single type of binding site available. Contrarily, a non-linear plot suggests heterogeneity and multiple binding sites (Anirudhan and Suchithra, 2010).

Figure 10 shows the Scatchard plots obtained for the adsorption of target species. It is evident from the plots that the adsorption

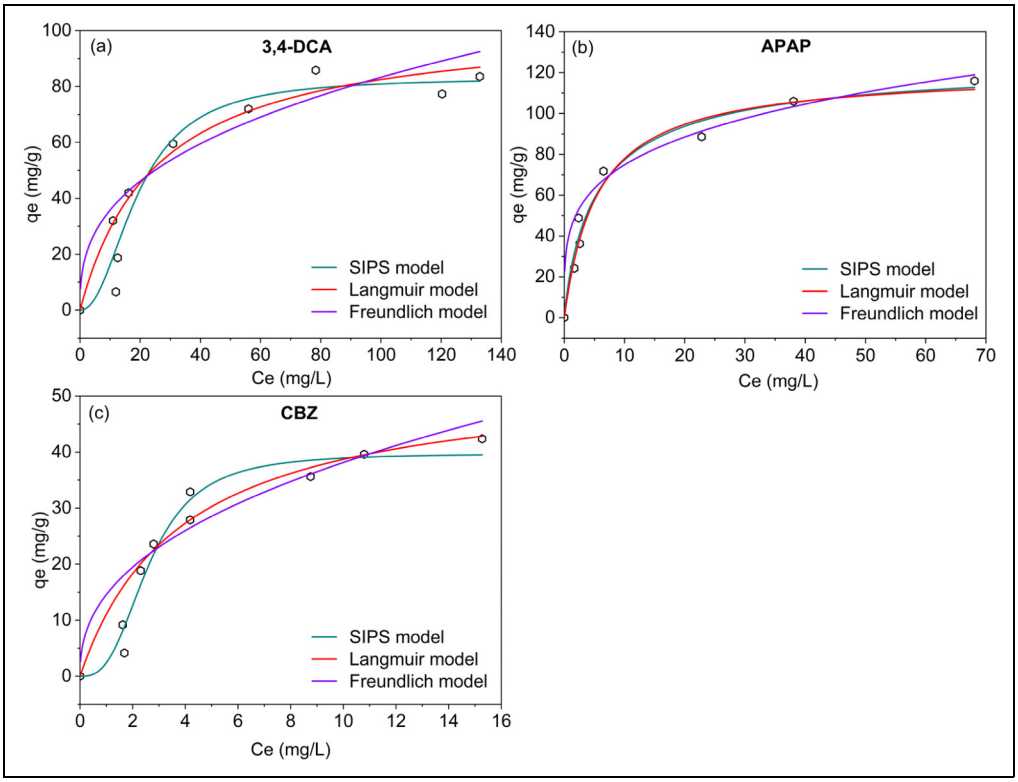

Figure 9. Adsorption isotherm models showing non-linear fits for (a) 3,4-DCA, (b) acetaminophen and (c) carbamazepine.

behaviour deviates from linearity. The high and low binding affinities can be attributed to the presence of more than one type of binding site, offering strong and weak interactions, respectively. The high affinity binding sites can be attributed to chemical interactions between the biochar surface and the target compounds whereas the low affinity sites indicate weak physical bonds. The plots further supplement the observations from Sips isotherm indicating a heterogeneous material with multiple binding sites.

Discussion

The results obtained suggest potential for application of the optimised biochar in water remediation, targeting persistent organic pollutants. The biochar surface area was higher than those reported for many wood-based biochars reported in the literature (Bataillou et al., 2022; Idowu and Fletcher, 2020). The sample presents a mixed microporous–mesoporous structure, as observed from the nitrogen isotherms with an average pore width of 4 nm, indicating that the mesopores present in the sample are narrow. Biochars pyrolysed at higher temperatures are linked with alkaline surface character (Shaheen et al., 2019), which fits with the PZC value obtained for the biochar produced at 725 °C (7.44 ± 0.2). FTIR analysis suggested a layered carbon structure with the presence of oxygen and nitrogen chemical moieties. These findings were further assisted by XPS analysis presenting a graphene-like arrangement, and 80% atomic carbon fraction. Additionally, the presence of oxygen and nitrogen-based functionalities was confirmed

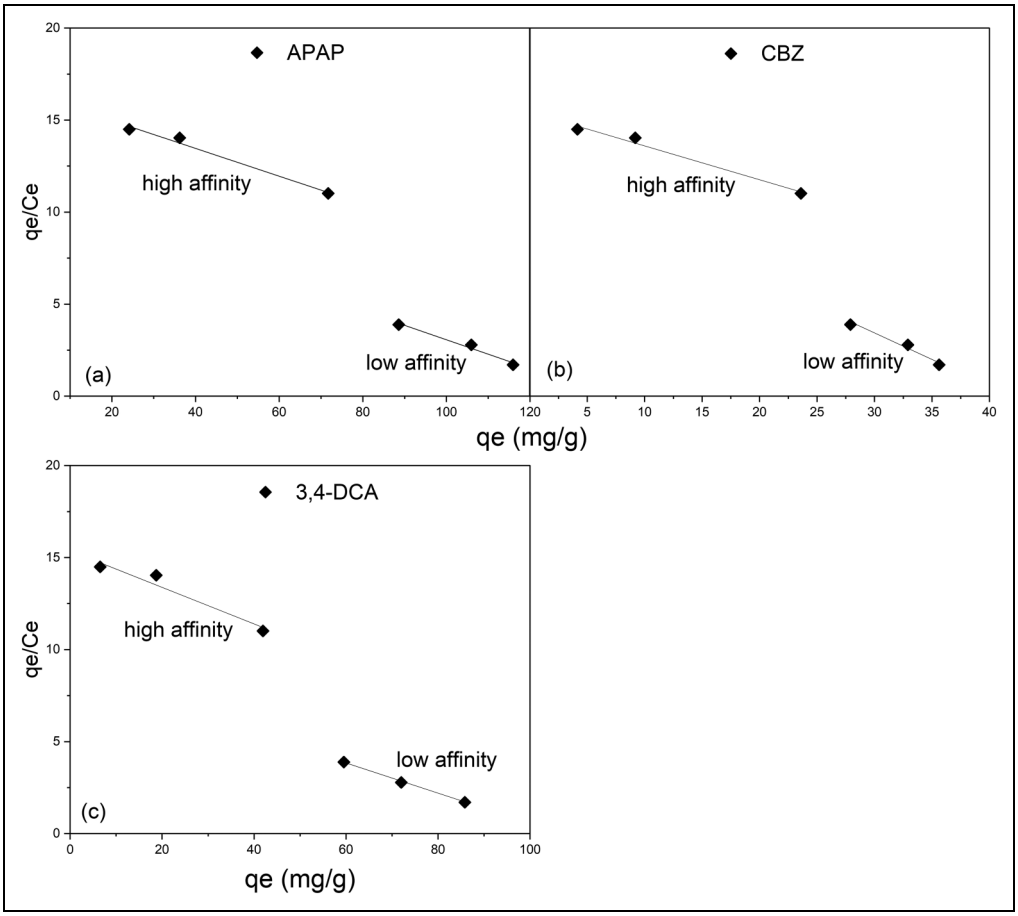

Figure 10. Scatchard plots for (a) APAP, (b) CBZ and (c) 3,4-DCA to determine the nature of binding sites on the biochar surface. Graph shows clear distinction between affinity zones suggesting heterogeneous surface.

from XPS data. These chemical moieties assist the hydrophilic nature of the biochar and provide a potential avenue for application in water remediation.

The application of biochar against 3,4-DCA, APAP and carbamazepine resulted in efficient removal of the species from an aqueous system. 3,4-DCA removal was characterised with fast removal rates and a very short equilibrium time of around 6 min and a maximum adsorption capacity of 83 mg/g. Although the maximum removal capacity was lower than some activated carbons reported in the literature, adsorption rates were far superior in achieving acceptable removal overall (Bakhaeva et al., 2001). Adsorption of APAP and CBZ was best explained by the linearised pseudo-second-order model indicating the formation of chemical bonds as the rate-limiting step. The maximum adsorption capacities for APAP and CBZ were 126 and 40 mg/g, respectively, and these were superior or on par with those reported in Table 4. The presence of nitrogen and oxygen functionalities on the surface of the biochars presents possible hydrogen bonding or π–π interactions between the benzene rings in the target elements and the biochar surface, as a possible removal

Table 4. Maximum uptake capacities of different adsorbents for Acetaminophen (APAP), carbamazepine (CBZ) and 3,4-DCA.

Adsorbent	Species	q_{max} (mg/g)	Adsorbent dosage	Initial concentration	Equilibrium time	Ref.
AC from wood	APAP	87	Fixed bed	1 g/L	2 h	Quesada-Peñate et al. (2012)
AC from coconut shell	APAP	135	Fixed bed	1 g/L	2 h	Quesada-Peñate et al. (2012)
AC from orange peels	APAP	118	0.25–1.25 g/L	20–150 mg/L	1.5 h	El Saied et al. (n.d.)
Biochar from Scottish softwood	APAP	126	2 g/L	25–300 mg/L	6 h	This study
Peanut shells biochar	CBZ	4.96	1:200 solid to aqueous	1–50 mg/L	168 h	Chen et al. (2017)
Pine sawdust biochar	CBZ	5.25	–	1–50 mg/L	168 h	Chu et al. (2019)
AC from Argan tree nutshells	CBZ	71.4	0.1 g/L	50 mg/L	2 h	El Mouchtari et al. (2020)
Biochar from Scottish softwood	CBZ	40	2 g/L	10–100 mg/L	24 h	This study
Kaolinite	3,4-DCA	0.311	20 g/L	10–200 mg/L	96 h	Luca Tasca and Fletcher (2017)
Montmorillonite	3,4-DCA	0.077	20 g/L	10–200 mg/L	96 h	Luca Tasca and Fletcher (2017)
Greenhouse biomass fly ash	3,4-DCA	0.125	20 g/L	1–5 mg/L	24 h	Quirantes et al. (2017)
Biochar from Scottish softwood	3,4-DCA	83	2 g/L	25–300 mg/L	0.16 h	This study

mechanism. Overall, the optimised biochar sample selected for application from the design of experiments optimisation study conducted previously (Jamal and Fletcher, 2023), provided fast adsorption kinetics and high adsorption capacities against the identified target molecules. The results provide an attractive avenue for biochar application for water remediation targeting a range of pollutants in aqueous media.

Conclusions

The optimised biochar produced from Scottish softwood showed good performance against selected pollutant species. The material was characterised with a high surface area and mixed microporous/mesoporous nature. Point of zero charge analysis indicated a neutral surface charge and X-ray photoelectron spectroscopy data suggested a hydrophilic nature and potential for application in water remediation. The material showed great performance against 3,4-dichloroaniline with rapid equilibrium proving difficult to perform a kinetic analysis. For acetaminophen and carbamazepine, adsorption followed a pseudo-second-order kinetic model. Adsorption isotherms were best explained by the Sips model for all three species suggesting the formation of an initial

monolayer with chemical bonding as the rate-limiting step. The highest adsorption capacity was noted in the case of acetaminophen. Scatchard plots suggested a heterogeneous surface with multiple binding sites. Ultimately, the results indicate a potential application of softwood biochar as a renewable adsorbent in water remediation.

Declaration of conflicting interests

The authors declared no potential conflicts of interest with respect to the research, authorship, and/or publication of this article.

Funding

The authors received no financial support for the research, authorship, and/or publication of this article.

Data availability statement

All data generated in this study are included in this article. No AIF-related data were generated in this study.

ORCID iD

Mohammad Umair Jamal https://orcid.org/0000-0001-5005-5817

Supplemental material

Supplemental material for this article is available online.

References

Abd N, Youssef E, Amer E, et al. (2020) Molten salt synthesis of hierarchically porous carbon for the efficient adsorptive removal of sodium diclofenac from aqueous effluents. https://doi.org/10.1016/j.jtice.2020.07.018.

Angın D (2013) Effect of pyrolysis temperature and heating rate on biochar obtained from pyrolysis of safflower seed press cake. *Bioresour Technol* 128: 593–597.

Angioi S, Polati S, Roz M, et al. (2005) Sorption studies of chloroanilines on kaolinite and montmorillonite. *Environmental Pollution* 134: 35–43.

Anirudhan TS and Suchithra PS (2010) Equilibrium, kinetic and thermodynamic modeling for the adsorption of heavy metals onto chemically modified hydrotalcite. *Indian Journal of Chemical Technology* 17: 247–259.

Azizian S (2004) Kinetic models of sorption: A theoretical analysis. *J Colloid Interface Sci* 276: 47–52.

Bakatula EN, Richard D, Neculita CM, et al. (2018) Determination of point of zero charge of natural organic materials. *Environmental Science and Pollution Research* 25: 7823–7833.

Bakhaeva LP, Vasilyeva GK, Surovtseva EG, et al. (2001) Microbial degradation of 3,4-dichloroaniline sorbed by activated carbon. *Microbiology (N Y)* 70: 277–284.

Barrett EP, Joyner LG and Halenda PP (1951) The determination of pore volume and area distributions in porous substances. I. Computations from nitrogen isotherms. *J Am Chem Soc* 73: 373–380.

Bataillou G, Lee C, Monnier V, et al. (2022) Cedar wood-based biochar: Properties, characterization, and applications as anodes in microbial fuel cell. *Appl Biochem Biotechnol* 194: 4169–4186.

Beamson G and Briggs D (1992) High resolution XPS of organic polymers: The scienta ESCA300 database. *J Chem Educ* 70: A25.

Bolong N, Ismail AF, Salim MR, et al. (2009) A review of the effects of emerging contaminants in wastewater and options for their removal. *Desalination* 239: 229–246.

Brunauer S, Emmett PH and Teller E (1938) Adsorption of gases in multimolecular layers. *J Am Chem Soc* 60: 309–319.

Burton GA Jr and Pitt R (2001) Stormwater Effects Handbook : A Toolbox for Watershed Managers, Scientists, and Engineers, Stormwater Effects Handbook. https://doi.org/10.1201/9781420036244.

Cao W, Li J, Lin L, et al. (2021) Release of potassium in association with structural evolution during biomass combustion. *Fuel* 287: 119524.

Chen J, Zhang D, Zhang H, et al. (2017) Fast and slow adsorption of carbamazepine on biochar as affected by carbon structure and mineral composition. *Science of The Total Environment* 579: 598–605.

Chu G, Zhao J, Liu Y, et al. (2019) The relative importance of different carbon structures in

biochars to carbamazepine and bisphenol A sorption. *J Hazard Mater* 373: 106–114.

Crisp TM, Clegg ED, Cooper RL, et al. (1998) Environmental endocrine disruption: An effects assessment and analysis. *Environ Health Perspect* 106: 11.

Décima MA, Marzeddu S, Barchiesi M, et al. (2021) A review on the removal of carbamazepine from aqueous solution by using activated carbon and biochar. *Sustainability* 13: 11760.

Ellappan P and Miranda LR (2014) Two-regime kinetic study and parameter optimization of degradation of 3,4-dichloroaniline using TI–N/S catalyst under visible light. *New Pub: Balaban* 57: 2203–2216.

El Mouchtari EM, Daou C, Rafqah S, et al. (2020) TiO_2 and activated carbon of Argania Spinosa tree nutshells composites for the adsorption photocatalysis removal of pharmaceuticals from aqueous solution. *J Photochem Photobiol A Chem* 388: 112183.

El Saied M, Shaban SA, Mostafa MS, et al. (n.d.) Efficient adsorption of Acetaminophen from the aqueous phase using low-cost and renewable adsorbent derived from orange peels. *Biomass Convers Biorefin* 1: 3.

Freundlich H (1907) Über die adsorption in lösungen. *Zeitschrift Für Physikalische Chemie* 57U: 385–470.

Gómez-Gualdrón DA, Moghadam PZ, Hupp JT, et al. (2016) Application of consistency criteria to calculate BET areas of micro- and mesoporous metal–organic frameworks. *J Am Chem Soc* 138: 215–224.

Harvey JK (n.d.) Pollution sources: Point and nonpoint – river, temperature, important, salt, types, system, plants, oxygen, human, Water Encyclopedia. Available at: http://www.waterencyclopedia.com/Po-Re/Pollution-Sources-Point-and-Nonpoint.html (accessed 11 July 2023).

He Y, Dong Y, Huang W, et al. (2015) Investigation of boron-doped diamond on porous ti for electrochemical oxidation of Acetaminophen pharmaceutical drug. *Journal of Electroanalytical Chemistry* 759: 167–173.

Ho YS and McKay G (1998) Sorption of dye from aqueous solution by peat. *Chemical Engineering Journal* 70: 115–124.

Huguenot D, Bois P, Jézéquel K, et al. (2010) Selection of low cost materials for the sorption of copper and herbicides as single or mixed compounds in increasing complexity matrices. *J Hazard Mater* 182: 18–26.

Ibrahim MA, Zulkifli SZ, Azmai MNA, et al. (2021) Reproductive toxicity of 3,4-dichloroaniline (3,4-DCA) on Javanese Medaka (Oryzias javanicus, Bleeker 1854). *Animals (Basel)* 11: 1–12.

Idowu GA and Fletcher AJ (2020) The manufacture and characterisation of rosid angiosperm-derived biochars applied to water treatment. *Bioenergy Res* 13: 387–396.

International Energy Agency (2017) Water-Energy Nexus, Paris. Available at: https://www.iea.org/reports/water-energy-nexus.

Iwuozor KO (2019) Prospects and challenges of using coagulation-flocculation method in the treatment of effluents. *Advanced Journal of Chemistry-Section A*: 105–127. https://doi.org/10.29088/sami/ajca.2019.2.105127.

Jamal MU and Fletcher AJ (2023) Design of experiments study on Scottish wood biochars and process parameter influence on final biochar characteristics. *Bioenergy Res* 1: 1–14.

Jiang H, Li X and Dai Y (2024) Phosphoric acid activation of cow dung biochar for adsorbing enrofloxacin in water: Icing on the cake. *Environmental Pollution* 341: 122887.

Jin X, Liu R, Wang H, et al. (2022) Functionalized porous nanoscale Fe_3O_4 particles supported biochar from peanut shell for Pb(II) ions removal from landscape wastewater. *Environmental Science and Pollution Research* 29: 37159–37169.

Jindo K, Mizumoto H, Sawada Y, et al. (2014) Physical and chemical characterization of biochars derived from different agricultural residues. *Biogeosciences* 11: 6613–6621.

Juárez R, Karlsson S, Falås P, et al. (2021) Integrating dissolved and particulate matter into a prediction tool for ozonation of organic micropollutants in wastewater. *Science of The Total Environment* 795: 148711.

Klamerth N, Rizzo L, Malato S, et al. (2010) Degradation of fifteen emerging contaminants at µg L−1 initial concentrations by mild solar

photo-Fenton in MWTP effluents. *Water Res* 44: 545–554.

Kloss S, Zehetner F, Dellantonio A, et al. (2012) Characterization of slow pyrolysis biochars: Effects of feedstocks and pyrolysis temperature on biochar properties. *J Environ Qual* 41: 990–1000.

Langmuir I (1916) The constitution and fundamental properties of solids and liquids. Part I. Solids. *J Am Chem Soc* 38: 2221–2295.

Larson AM, Polson J, Fontana RJ, et al. (2005) Acetaminophen-induced acute liver failure: Results of a United States multicenter, prospective study. *Hepatology* 42: 1364–1372.

Lee JW, Kidder M, Evans BR, et al. (2010) Characterization of biochars produced from cornstovers for soil amendment. *Environ Sci Technol* 44: 7970–7974.

Lhoest JB, Bertrand P, Weng LT, et al. (1995) Combined time-of-flight secondary Ion mass spectrometry and X-ray photoelectron spectroscopy study of the surface segregation of poly(-methyl methacrylate) (PMMA) in bisphenol a polycarbonate/PMMA blends. *Macromolecules* 28: 4631–4637.

Li W, Nanaboina V, Zhou Q, et al. (2012) Effects of Fenton treatment on the properties of effluent organic matter and their relationships with the degradation of pharmaceuticals and personal care products. *Water Res* 46: 403–412.

Liang G, Hu Z, Wang Z, et al. (2020) Effective removal of carbamazepine and diclofenac by CuO/Cu_2O/Cu-biochar composite with different adsorption mechanisms. *Environ Sci Pollut Res Int* 27: 45435–45446.

Lippens BC and de Boer JH (1965) Studies on pore systems in catalysts: V. The t method. *J Catal* 4: 319–323.

Liu Y and Shen L (2008) From Langmuir kinetics to first- and second-order rate equations for adsorption. *Langmuir* 24: 11625–11630.

Livingston AG and Willacy A (1991) Degradation of 3,4-dichloroaniline in synthetic and industrially produced wastewaters by mixed cultures freely suspended and immobilized in a packed-bed reactor. *Appl Microbiol Biotechnol* 35: 551–557.

Loos R, Carvalho R, António DC, et al. (2013) EU-wide monitoring survey on emerging polar organic contaminants in wastewater treatment plant effluents. *Water Res* 47: 6475–6487.

López GP, Castner DG and Ratner BD (1991) XPS O1s binding energies for polymers containing hydroxyl, ether, ketone and ester groups. *Surface and Interface Analysis* 17: 267–272.

Luca Tasca A and Fletcher A (2017) State of the art of the environmental behaviour and removal techniques of the endocrine disruptor 3,4-dichloroaniline. *Journal of Environmental Science and Health, Part A Toxic/Hazardous Substances and Environmental Engineering*. https://doi.org/10.1080/10934529.2017.1394701.

Matta R, Tlili S, Chiron S, et al. (2011) Removal of carbamazepine from urban wastewater by sulfate radical oxidation. *Environ Chem Lett* 9: 347–353.

Moussout H, Ahlafi H, Aazza M, et al. (2018) Critical of linear and nonlinear equations of pseudo-first order and pseudo-second order kinetic models. *Karbala International Journal of Modern Science* 4: 244–254.

Nandiyanto ABD, Oktiani R and Ragadhita R (2019) How to read and interpret FTIR spectroscope of organic material. *Indonesian Journal of Science and Technology* 4: 97.

NIST X-ray Photoelectron Spectroscopy (XPS) Database, Version 3.5 (n.d.) Available at: https://srdata.nist.gov/xps/ (accessed 1 August 2023).

Nurul M, Bhuiyan H, Kang H, et al. (2021) Effects of 3,4-dichloroaniline (3,4-DCA) and 4,4 0-methylenedianiline (4,4 0-MDA) on sex hormone regulation and reproduction of adult zebrafish (*Danio rerio*). *Chemosphere* 269: 128768.

Oladipo AA and Mustafa FS (2023) Bismuth-based nanostructured photocatalysts for the remediation of antibiotics and organic dyes. *Beilstein Journal of Nanotechnology* 14(26): 291–321.

Oladipo AA, Mustafa FS, Ezugwu ON, et al. (2022) Efficient removal of antibiotic in single and binary mixture of nickel by electrocoagulation process: Hydrogen generation and cost analysis. *Chemosphere* 300: 134532.

Pauletto PS, Lütke SF, Dotto GL, et al. (2021) Adsorption mechanisms of single and simultaneous removal of pharmaceutical compounds

onto activated carbon: Isotherm and thermodynamic modeling. *J Mol Liq* 336: 116203.

Phong Vo HN, Le GK, Hong Nguyen TM, et al. (2019) Acetaminophen Micropollutant: Historical and current occurrences, toxicity, removal strategies and transformation pathways in different environments. *Chemosphere* 236: 124391.

Polati S, Gosetti F, Gianotti V, et al. (2006) Sorption and desorption behavior of chloroanilines and chlorophenols on montmorillonite and kaolinite. *J Environ Sci Health B* 41: 765–779.

Qiu M, Hu B, Chen Z, et al. (2021) Challenges of organic pollutant photocatalysis by biochar-based catalysts. *Biochar* 3: 117–123.

Qiu M, Liu L, Ling Q, et al. (2022) Biochar for the removal of contaminants from soil and water: A review. *Biochar* 4: 1–25.

Quesada-Peñate I, Julcour-Lebigue C, Jáuregui-Haza UJ, et al. (2012) Degradation of paracetamol by catalytic wet air oxidation and sequential adsorption – catalytic wet air oxidation on activated carbons. *J Hazard Mater* 221–222: 131–138.

Quirantes M, Nogales R and Romero E (2017) Sorption potential of different biomass fly ashes for the removal of diuron and 3,4-dichloroaniline from water. *J Hazard Mater* 331: 300–308.

Reddygunta KKR, Callander A, Šiller L, et al. (2022) Sono-exfoliated graphene-like activated carbon from hazelnut shells for flexible supercapacitors. *Int J Energy Res* 46: 16512–16537.

Rizzo L, Malato S, Antakyali D, et al. (2019) Consolidated vs new advanced treatment methods for the removal of contaminants of emerging concern from urban wastewater. *Science of The Total Environment* 655: 986–1008.

Rodriguez-Narvaez OM, Peralta-Hernandez JM, Goonetilleke A, et al. (2017) Treatment technologies for emerging contaminants in water: A review. *Chemical Engineering Journal* 323: 361–380.

Shaheen SM, Niazi NK, Noha E, et al. (2019) Wood-based biochar for the removal of potentially toxic elements in water and wastewater: A critical review. *International Materials Reviews* 64: 216–247.

Shard AG (2020) Practical guides for x-ray photoelectron spectroscopy: Quantitative XPS. *Journal of Vacuum Science & Technology A: Vacuum, Surfaces, and Films* 38: 41201.

Sing KSW (2014) 7 – assessment of surface area by gas adsorption. In: Rouquerol F, Rouquerol J, Sing KSW, Llewellyn P and Maurin G (eds) *Adsorption by Powders and Porous Solids*, 2nd ed. Oxford: Academic Press, pp.237–268. https://doi.org/10.1016/B978-0-08-097035-6.00007-3.

Sips R (1948) On the structure of a catalyst surface. *J Chem Phys* 16: 490–495.

Smith KL and Black KM (1984) Characterization of the treated surfaces of silicon alloyed pyrolytic carbon and SiC. *Journal of Vacuum Science & Technology A* 2: 744–747.

Su CC, Cada CA, Dalida MLP, et al. (2013) Effect of UV light on Acetaminophen degradation in the electro-Fenton process. *Sep Purif Technol* 120: 43–51.

Svenska Vetenskapsakademiens SL-K (n.d.) Handlingar, undefined 1898, Zur theorie der sogenannten adsorption geloster stoffe, Cir.Nii.Ac.Jp. Available at: https://cir.nii.ac.jp/crid/1572824501080908544 (accessed 17 July 2023).

Thommes M, Kaneko K, Neimark AV, et al. (2015) IUPAC Technical Report Physisorption of gases, with special reference to the evaluation of surface area and pore size distribution (IUPAC Technical Report). https://doi.org/10.1515/pac-2014-1117.

Tran HN, Tomul F, Thi Hoang Ha N, et al. (2020) Innovative spherical biochar for pharmaceutical removal from water: Insight into adsorption mechanism. *J Hazard Mater* 394: 122255.

United Nations Educational Scientific and Cultural Organization (2021) The United Nations World Water Development Report 2021: Valuing water, Water Politics, 206. Available at: https://unesdoc.unesco.org/ark:/48223/pf0000375724 (accessed 10 July 2023).

van Oss CJ (2007) A review of: "active carbon." R.C. Bansal, J.B. Donnet and F. Stoeckli; Marcel Dekker, New York, 1988. pp. 482, $135.00. *Http://Dx.Doi.Org/10.1080/01932699008943255* 11: 323–323.

Vaseashta A (2009) Nanomaterials for Chemical—Biological—Physical Integrity of Potable Water, 1–16. https://doi.org/10.1007/978-90-481-3497-7_1.

Verla AW, Enyoh CE, Verla EN, et al. (2019) Microplastic–toxic chemical interaction: A review study on quantified levels, mechanism and implication. *SN Appl Sci* 1: 1–30.

Wagener K, Batich C, Kirsch B, et al. (1989) Chain propagation/step propagation polymerization. III. An XPS investigation of poly(oxyethylene)-b-poly(pivalolactone) telechelomer. *J Polym Sci A Polym Chem* 27: 2625–2631.

Wang J and Guo X (2020a) Adsorption isotherm models: Classification, physical meaning, application and solving method. *Chemosphere* 258: 127279.

Wang J and Guo X (2020b) Adsorption kinetic models: Physical meanings, applications, and solving methods. https://doi.org/10.1016/j.jhazmat.2020.122156.

Wang Y, Lin C, Liu X, et al. (2021) Efficient removal of acetochlor pesticide from water using magnetic activated carbon: Adsorption performance, mechanism, and regeneration exploration. *Science of The Total Environment* 778: 146353.

Weber TW and Chakravorti RK (1974) Pore and solid diffusion models for fixed-bed adsorbers. *AIChE Journal* 20: 228–238.

Weber WJ (1974) Adsorption processes. *Pure and Applied Chemistry* 37: 375–392.

Weber WJ Jr and Morris JC (1963) Kinetics of adsorption on carbon from solution. *Journal of the Sanitary Engineering Division* 89: 31–59.

Zhang H, Voroney RP and Price GW (2015) Effects of temperature and processing conditions on biochar chemical properties and their influence on soil C and N transformations. *Soil Biol Biochem* 83: 19–28.

Zhao Z, Sun W and Ray MB (2022) Adsorption isotherms and kinetics for the removal of algal organic matter by granular activated carbon. *Science of The Total Environment* 806: 150885.